DOI: 10.26599/FSHW.2026.9251286

Contents lists available at SciOpen

Food Science and Human Wellness

journal homepage: https://www.sciopen.com/journal/2097-0765

China Food Publishing Co.

Antibacterial mechanism of a multitarget antibacterial peptide CpAtt against *Staphylococcus aureus*

Yuhang Wang[a,b,1], Lingling Zhou[a,c,1], Xiangfeng Meng[a], Yayun Jiao[a], Shengming Ma[a,c], Yuanchen Zhang[a], Zengjun Ma[b*], Kaiqi Lian[a,c*]

[a.] *School of Biotechnology and Food Science, Anyang Institute of Technology, Anyang 455000, China*

[b.] *College of Animal Science and Technology, Hebei Normal University of Science and Technology, Qinhuangdao 066004, China*

[c.] *Henan Joint International Research Laboratory of Veterinary Biologics Research and Application, Anyang 455000, China.*

ABSTRACT: *Staphylococcus aureus* (*S. aureus*) poses a serious threat to food safety and global health, driving the demand for natural and safe antimicrobials. CpAtt, an attacin-like antimicrobial peptide identified previously in our laboratory, demonstrated potent antibacterial activity against *S. aureus*. This study systematically elucidated the multi-target antibacterial mechanisms of CpAtt against *S. aureus*. The bacteriostatic curve confirmed that 1 MIC CpAtt effectively inhibited the *S. aureus* proliferation within 12 h. CpAtt disrupted cell wall and membrane integrity in *S. aureus*, as evidenced by blurred ultrastructure features, and significant leakage of nucleic acids, proteins, alkaline phosphatase, and β-galactosidase. Increased propidium iodide uptake increase further indicated that CpAtt increased cell membrane permeability. Transcriptomic analysis revealed that CpAtt disrupts multiple physiological processes. Specifically, these genes involved in the peptidoglycan biosynthesis pathway, the accessory gene regulator system, the TCA cycle, and succinate dehydrogenase were downregulated, whereas genes encoding for F-type ATPase, Cytochrome c oxidase, and Cytochrome bd complex were upregulated. Consequently, intracellular ATP levels dropped significantly, while reactive oxygen species levels decreased, suggesting that CpAtt impaired the energy metabolismwithout inducing the oxidative damage. *In vitro* binding assays and molecular docking analyses indicated that CpAtt interacts with genomic DNA primarily through electrostatic interactions between its positively charged residues and the anionic phosphate backbone. Notably, at sub-inhibitory concentrations, CpAtt modulated the transcription of adhesion-related genes in *S. aureus*, thereby suppressing biofilm formation. Consistently, *in vivo* experiments preliminarily demonstrated that CpAtt promotes skin wound healing in mice while conferring protection against infection when administered at appropriate doses. Collectively, these findings indicated that the antibacterial activity of CpAtt on *S. aureus* involves multiple targets, offering a strategic basis for the development of novel preservatives and antibacterial agents.

Keywords: Antimicrobial peptides; *Staphylococcus aureus*; Cell membrane; Energy metabolism; Biofilm

1. Introduction

Staphylococcus aureus (*S. aureus*) is a common zoonotic pathogen that frequently exists as part of the normal microbial flora in the oral and nasal cavities and on the skin of humans and warm-blooded

[1] These authors contributed equally to this work.
*** Corresponding authors.**
liankaiqi616@163.com (K.Q. Lian); mzj6699@126.com (Z.J. Ma)

Received 27 January 2026
Received in revised from 6 March 2026
Accepted 11 May 2026

mammals[1-2]. Its clinical significance is underscored by the production of various toxins that cause bacteremia, endocarditis, and pneumonia[3]. In addition, *S. aureus* can contaminate various foods including dairy products, meat, seafood, and ready-to-eat items, leading to food poisoning through the production of enterotoxins[4-5]. For example, the Chinese Center for Disease Control and Prevention recently reported an outbreak of foodborne illness at a hotel in Henan Province, China, where 14 individuals developed nausea, vomiting, and diarrhea after attending a banquet. The outbreak was attributed to *S. aureus* contamination of the donkey meat and goose meat they consumed[6]. Currently, most approaches for inhibiting *S aureus* proliferation rely on broad-spectrum antibiotics and chemical disinfectants. These strategies typically target a single key factor essential for bacterial survival, such as enzymes involved in cell wall synthesis or nucleic acid metabolism. However, under such single-target regimens, pathogenic bacteria like *S. aureus* can readily develop resistance through point mutations, modification of target sites, or upregulation of efflux pumps, facilitating the rapid spread of clinical drug resistance. It has been estimated that nearly 5 million deaths in 2019 were attributable to bacterial resistance, and the burden attributed to *S. aureus* was second only to that of *Escherichia coli* (*E. coli*)[7]. Additionally, *S. aureus* can adhere to various biotic and abiotic surfaces and become embedded within extracellular polymeric substances (EPS) to form biofilms, which can develop on various food-processing equipment or food surfaces. This not only promotes cross-contamination but also forms a physical barrier, significantly reducing the effective penetration concentration of the antibacterial agents. Even when small amounts of the drug penetrate, deeply dormant bacteria can still survive its bactericidal effect[8-9]. These two antimicrobial resistance mechanisms often coexist in clinical infections, further compromising the efficacy of traditional single-target antibacterial agent. Therefore, given the safety controversies surrounding traditional chemical preservatives and the growing trend toward restricting antibiotic use, there is an urgent need to develop novel antimicrobial agents that are natural, safe, and exhibit multi-target antibacterial activity[10].

Antimicrobial peptides (AMPs) have garnered widespread attention owing to their broad-spectrum activity and low propensity to induce drug resistance, and are regarded as one of the most promising "alternatives to antibiotics" in the field of food preservation[11]. As of September 2025, the Antimicrobial Peptide Database (https://aps.unmc.edu/) has cataloged 3,351 natural AMPs, of which host defense peptides from animals account for 76% of the total, including 397 AMPs from insects[10, 12]. AMPs typically consist of 10-100 amino acids, and most AMPs carry a net positive charge ranging from +2 to +9. This allows them to interact with the negatively charged phospholipid bilayer of bacteria, altering membrane permeability and ultimately causing membrane rupture and leakage of cellular contents. This is the most widespread bactericidal mechanism[13]. Moreover, they often possess intracellular targeting functions such as interfering with intracellular protein synthesis, inhibiting cell wall synthesis, and disrupting intracellular metabolism, thereby inhibiting bacterial growth[14, 16]. These effects differ from the single target of traditional antibiotics; they are less likely to select for resistance-conferring mutations. Therefore, AMPs represent an important strategy for developing alternatives to antibiotics and chemical preservatives.

Among the diverse families of AMPs, attacins represent a glycine-rich subclass derived from the humoral immunity of arthropods. Although often characterized as cationic AMPs, their net charge ranges from -3 to +10, suggesting that overall charge may not be the primary determinant of their antibacterial activity[17]. Attacins were initially believed to be effective only against Gram-negative bacteria such as *E. coli*[18-20]. However, subsequent research proved that some attacins also exert inhibitory effects against Gram-positive bacteria[21, 22]. Like most AMPs, attacins can target the bacterial outer membrane. For instance, Carlsson et al.[18, 20] reported that an attacin from the *Hyalophora cecropia* inhibited the synthesis of outer membrane proteins in *E. coli* by interfering with the transcription of the *omp* gene, thereby affecting the permeability of the outer membrane. Subsequently, they found that this attacin did not need to enter the inner membrane or cytoplasm of *E. coli*, but rather affected lipopolysaccharide synthesis by simply contacting lipopolysaccharide on the bacterial surface, and induced the production of intracellular stress proteins[23]. Fahmy et al.[24] reported that an attacin from *Hermetia illucens* could also disrupt the outer membrane of bacteria and further demonstrated that its destructive capacity on the outer membrane of *Pseudomonas aeruginosa* was greater than that of the clinically relevant antibiotic polymyxin. Nevertheless, the antibacterial mechanism of attacins against Gram-positive bacteria remains largely unknown, with only limited reports documenting their antibacterial activity[17, 21, 22]. In a previous study, we identified and characterized an attacin (designated CpAtt) from *Conogethes punctiferalis*[25]. CpAtt adopts a β-barrel fold with electrostatic heterogeneity, and exhibited more pronounced inhibitory effects against Gram-positive bacteria[25]. However, it remains unclear the precise antibacterial mechanism of CpAtt against *S. aureus* has remained. Therefore, the present study employed complementary approaches to elucidate the antibacterial mechanism of CpAtt against *S. aureus*, thereby advancing our understanding of how attacins exert their effects against Gram-positive bacteria.

2. Materials and methods

2.1 Bacterial strain and culture conditions

S. aureus CMCC(B) 26003 was maintained at the Henan Joint International Research Laboratory of Veterinary Biologics Research and Application at Anyang Institute of Technology (Anyang, China). *S. aureus* suspension were inoculated separately into Luria-Bertani (LB) broth and incubated overnight at 37 ℃.

2.2 Bacteriostatic curve

S. aureus cultures in the logarithmic growth phase were diluted 1:100 into sterile LB broth. CpAtt was added to these cultures to achieve final concentrations corresponding to 0, 1, 2, and 4 MIC, respectively. The treated cultures were then incubated at 37 °C for 24 h. At specified time intervals (0, 2, 4, 6, 8, 10, 12, and 24 h), 100 μL aliquots were collected from each group. The optical density at 600 nm for each aliquot was subsequently measured using an automated microplate reader (Synergy H1, BioTek, USA).

2.3 Time-kill assay

The killing kinetics of CpAtt against *S. aureus* were determined. Briefly, *S. aureus* cultures in the logarithmic growth phase were diluted 1:100 in sterile LB broth. CpAtt was then added to the cultures to

achieve final concentrations of 0, 1, 2, and 4 MIC. Vancomycin was added at final concentrations of 1 MIC (1 μg/mL) and 4 MIC (4 μg/mL) as positive controls. The treated cultures were incubated at 37 °C for 12 h. At 0, 6, and 12 hours, 100 μL of each bacterial culture was removed, resuspended in PBS, and serially diluted. The dilutions were then spotted onto LB agar plates. After overnight incubation at 37 °C, colony counts were determined.

2.4 Transmission electron microscope (TEM)

S. aureus cells in the logarithmic growth phase were harvested by centrifugation at 6,000×*g* for 5 min at room temperature. The resulting bacterial precipitate was washed twice with PBS and reconstituted to its original volume in PBS. For the treatment group, CpAtt was added at a final concentration of 2 MIC, while an equivalent volume of PBS served as the negative control. The samples were incubated for 1 h at 37 °C, and then centrifuged again. The harvested cell pellet was then resuspended in a suitable fixative for electron-microscopy and fixed for 2 h at room temperature. Finally, the fixed samples were submitted to Wuhan Servicebio Technology Co., Ltd. (Wuhan, China) for subsequent processing and imaging, according to the established protocol in our laboratory[26].

2.5 Nucleic acids and protein leakage

S. aureus bacterial suspension was prepared as described in Section 2.4, CpAtt was added at a final concentration of 1, 2, 4 MIC, and an equal volume of PBS was added as a negative control. The samples were incubated in a 37 °C constant-temperature water bath. The bacterial suspension was collected every hour for 6 hours and centrifuged at 6,000×*g* for 5 min. An ultra-micro UV spectrophotometer (NanoDrop 2000, Thermo Fisher Scientific, USA) was used to measure OD_{260} and OD_{280} values of the supernatant[27].

2.6 Cell wall and membrane permeability measurement

All samples were prepared following the methodology outlined in section 2.5, with 0.3% (v/v) Triton X-100 serving as the positive control. All groups were incubated for 1 h in a water bath at 37 °C, and centrifuged (6,000×*g*, 5 min) to separate the supernatants from the bacterial pellets. The membrane integrity of *S. aureus* treated with CpAtt was subsequently assessed by measuring the leakage of alkaline phosphatase (ALP) and β-galactosidase, in conjunction with propidium iodide (PI) staining, as described in prior work[28].

For the ALP assay, the collected supernatant was combined with the working solution from an Alkaline Phosphatase Assay Kit (Beyotime, Shanghai, China) according to the manufacturer's protocol and incubated at 37 °C for 10 min. Absorbance at 405 nm was then recorded using an automated microplate reader (Synergy H1, BioTek, USA). The ALP activity was calculated based on a standard curve and the definition of enzyme activity units. Concurrently, β-galactosidase activity was determined by adding ONPG (Solarbio, Beijing, China) to the supernatant at a final concentration of 3 mM. After an 8 h incubation at 37 °C, the absorbance was measured at 420 nm. The sediment collected by centrifugation was washed with PBS and resuspended, after which PI staining solution (Beyotime, Shanghai, China) was added. The sample was incubated in the

dark at 37 °C for 30 min. Fluorescence intensity was measured using an automatic multi-function microplate reader at an excitation wavelength of 536 nm and an emission wavelength of 617 nm.

2.7 Transcriptomic analysis

S. aureus bacterial suspension was prepared as described in section 2.4, CpAtt was added at a final concentration of 1 MIC, and an equal volume of PBS was added as a negative control. The samples were incubated in a constant temperature water bath at 37 °C for 2 h[29]. The bacterial cultures were then washed twice with PBS and centrifuged at 6,000×g for 5 min at 4 °C to collect the bacterial pellets. RNA-Seq was performed using the Illumina platform (NovaSeq-PE150) at Novogene Co, Ltd. (Beijing, China). Total RNA was extracted from the samples, and quantified using NanoDrop 2000 and Agilent 5400 Bioanalyzer. RNA purity was assessed by agarose gel electrophoresis and the Agilent 5400 Bioanalyzer. An adjusted *P*-value (Padj, Student's t-test with Benjamini-Hochberg false discovery rate adjustment) < 0.05 and $|\log_2$ fold change$| > 1$ was applied as the cut-off for significantly differentially expressed genes (DEGs). The data were uploaded to the Novomagic cloud platform (https://magic.novogene.com) following database searching for data analysis.

2.8 Validation of RNA-Seq results by real-time quantitative polymerase chain reaction (RT-qPCR)

RT-qPCR was performed as reported by Li et al.[30] with minor modifications using the same *S. aureus* cell samples from RNA-seq analysis. Eight DEGs (*murA1*, *murD*, *agrA*, *agrB*, *agrC*, *agrD*, vraS, *vraR*) were selected from the pathways of interest, and RNA-seq findings were validated using the primers listed in Table 1. Relative expression was calculated by the 2^(-ΔΔCt) algorithm after obtaining Ct values[27].

Table 1 RT-qPCR primer sequences

Gene	Forward sequence (5'-3')	Reverse sequence (5'-3')
16S	GCTGCCCTTTGTATTGTC	AGATGTTGGGTTAAGTCC
murA1	CCACATCCTGGATTCCCGAC	GCGGCTGCTGCTCTTAAATC
murD	TGTGGTGGTTTGGATCGAGG	GCGTCTTCGACATTGTTCGC
agrA	CGTGGCAGTAATTCAGTGTATGTTC	TCTAAATGGGCAATGAGTCTGTGAG
agrB	TTGACCAGTTTGCCACGTATCTTC	AGCTAAGACCTGCATCCCTAATCG
agrC	CGCTGATGATATACCACGCATTC	TTGATAGACCTAAACCACGACCTTC
agrD	TAAAAAACATTGGTAACATCGCAG	CGTGTAATTGTGTTAATTCTTTTGG
vraS	GCGTTCAATGGAAGGCGAAA	GCCGCAAAAAGTTGCTGACT
vraR	GAAGCAATTGCCAAAGCCCA	TTTTACGAACTGCATCGGCG
icaA	TCGCACTCTTTATTGATAGTCGCT	CGACAAGAACTACTGCTGCGT
icaB	AGCAGTCACTCCGAACTCCA	TCATGGAATCCGTCCCATCTCT
icaD	ACTATGGGCATTTTCGCGATTATCA	ACGATTCTCTTCCTCTCTGCCAT

2.9 Adenosine triphosphate (ATP) measurement

All samples were processed as described in Section 2.5 and incubated in a 37 ℃ constant temperature water bath for 1 h. Referring to the method of Shi et al.[15], the effect on the *S. aureus* ATP content was determined using an enhanced ATP assay kit (Beyotime, Shanghai, China). Briefly, *S. aureus* was lysed under ice water bath conditions and then mixed with firefly luciferase and luciferin. After reacting at room temperature for 3 min, the luminescence intensity of the sample was measured using an automatic multi-function microplate reader (Synergy H1, BioTek, USA).

2.10 Reactive oxygen species (ROS) generation measurement

S. aureus bacterial suspension was prepared as described in Section 2.5, DCFH-DA was added at a final concentration of 10 μM. The samples were incubated at 37 ℃ for 20 min, washed three times with PBS, and then resuspended. *S. aureus* cells were subsequently treated with different concentrations of CpAtt (1, 2, and 4 MIC), while Rosup at a final concentration of 100 μg/mL was added as a positive control and incubated at 37 ℃. At 30 min, the fluorescence intensity of the samples were measured using an automatic multi-function microplate reader (Synergy H1, BioTek, USA) at an excitation wavelength of 488 nm and emission wavelength of 525 nm.

2.11 Agarose gel retardation experiment

Genomic DNA of *S. aureus* in the logarithmic growth phase was extracted using a bacterial DNA extraction kit (Sangon, Shanghai, China). Different quantities of CpAtt were added to 0.5 μg of genomic DNA to yield CpAtt-to-DNA mass ratios of 0, 0.5, 1, 2.5, 5, and 10. Incubations were carried out at 37 °C for 30 min in a water bath. The migration of genomic DNA was analyzed by agarose gel electrophoresis[31].

2.12 Molecular docking analysis

Molecular docking of CpAtt with DNA was performed using the HDOCK SERVER (http://hdock.phys.hust.edu.cn/)[32]. As described by Tao et al.[33], the DNA structure of *S. aureus* (ID: 2XCT) was downloaded from the PDB database, and ligands, water molecules, and hydrogens were removed. The 3D structure of CpAtt was previously constructed by AlphaFold v2.1.0[25]. Using DNA as the receptor and CpAtt as the ligand, the structures was uploaded to the HDOCK SERVER and docked employing the default hybrid docking strategy. The docking results were visualized using PyMOL v2.6.

2.13 Biofilm inhibition assay

The effect of CpAtt on *S. aureus* biofilm formation was evaluated using the crystal violet staining method as previously described[28]. Briefly, 10^7 CFU/mL *S. aureus* suspension was treated with CpAtt at concentrations equivalent to 1/4 and 1/2 MIC. A control group was treated with an equal volume of PBS instead. All samples were then incubated for 24 h at 37 °C in a humidified atmosphere. After incubation, planktonic bacteria were removed, and the biofilm was fixed with methanol, stained with 0.5% (v/v) crystal violet for 20 min, washed, and photographed using an inverted microscope (Zeiss, Oberkochen, Germany). The biofilm was solubilized completely with 33% acetic acid and diluted appropriately. The optical density at 600 nm was determined as a measure of biofilm mass.

2.14 Expression level measurement of biofilm-related genes

S. aureus suspension (1×10^7 CFU/mL) were treated with CpAtt at sub-inhibitory concentrations of 1/4 MIC and 1/2 MIC. A parallel control sample received an equivalent volume of PBS. All cultures were incubated for 24 h at 37 °C with shaking at 140 rpm. Then, total RNA was isolated from the bacterial cells using Trigene reagent (GenStar, Beijing, China), according to the manufacturer's instructions. Subsequently, 500 ng of the extracted RNA served as the template for first-strand cDNA synthesis, which was performed

using a TaKaRa PrimeScript™ II 1st Strand cDNA Synthesis Kit (TaKaRa, Beijing, China) as per the provided instructions. The transcriptional levels of the target genes (*icaA*, *icaB*, *icaD*, and *agrA*) were quantified via the method detailed in section 2.8 (see Table 1 for primers). The relative expression of each gene transcript was calculated using the 2^(-ΔΔCt) method, with the 16S rRNA gene serving as the endogenous control for normalization.

2.15 Mice Skin Wounds Infection Model

All animal experiments were approved by the Experimental Animal Management and Animal Welfare Ethics Committee of the College of Biology and Food Engineering, Anyang Institute of Technology (AGSWN202501). The therapeutic effect of CpAtt against *S. aureus* CMCC(B) 26003 was assayed in a wounded mice skin infection model. Female KM mice (30-33 g, randomly divided into 4 groups, 6 mice/group, 24 mice in total) were purchased from Sibefu (Beijing) Biotechnology Co., Ltd., China, and housed in a room with natural light, experiencing day and night alternations, and controlled temperature at (25 ± 1) ℃. Mice were provided with a commercial pellet diet and sterile distilled water *ad libitum*. After 7 days acclimation period to the environment, mice were anesthetized by intraperitoneal injection of pentobarbital (30 mg/kg). After which, the dorsal hair was removed with a shaver and depilatory cream, and a 10-mm-diameter full-thickness excisional wound was created with a biopsy punch. *S. aureus* suspension was prepared as described in Section 2.3. Each mouse in three groups was infected with 100 μL of bacterial suspension, resulting in 1×10^7 CFU per wound. The remaining group received an equal volume of PBS as a blank control. At 1 h post-infection, 50 μL of PBS was given to the wounds of the negative control group, and 50 μL of CpAtt (400 μg/mL or 200 μg/mL) was applied to the wounds the high concentration and low concentration treatment groups, respectively. Meanwhile, 50 μL PBS was given to the blank control group. PBS and CpAtt treatments were repeated after 24 h. Mice were monitored and photographed on days 0, 1, 3, 5, 7 and 14, and the wound areas were calculated with ImageJ. On the 3th day, the wound tissues of randomly selected three mice from each group were homogenized in 1 mL of sterile PBS and serial dilutions of the suspension were plated on LB agar plates (containing 7.5% sodium chloride), and incubated for 12 h. Moreover, on the 14th day, full-thickness skin samples around the wounds were excised and fixed in 4% tissue fixative solution (Servicebio, Wuhan, China) for 24 h. According to the experimental Standard Operation Procedure (SOP) of Servicebio (Wuhan, China), skin tissue sections were prepared and stained with hematoxylin-eosin (H&E) or Masson's trichrome stain[34]. Quantitative analysis of Masson staining was performed using ImageJ software.

2.16 Statistical analysis

Experimental data were analyzed and plotted using GraphPad Prism 10.5 (La Jolla, CA, USA). All experiments were performed in triplicate and data are expressed as the mean ± standard deviation. Statistical differences between groups were analyzed for significance using Student's *t*-tests or ordinary one-way ANOVA. $P < 0.05$ was considered statistically significant.

3. Results

3.1 Effects of CpAtt on the growth and mortality of S. aureus

The antibacterial activity of CpAtt against *S. aureus* at different growth stages was evaluated by measuring the bacteriostatic curves. Compared with the control group, treatment with 1 MIC (37.5 μg/mL) CpAtt significantly inhibited *S. aureus* growth within 12 hours, whereas 2 and 4 MIC CpAtt sustained growth inhibition for at least 24 hours (Fig. 1A). The bactericidal activity of CpAtt at different concentrations was also assessed. While 1 MIC CpAtt failed to effectively kill *S. aureus*, concentrations of 2 and 4 MIC exhibited a marked bactericidal effect (Fig. 1B).

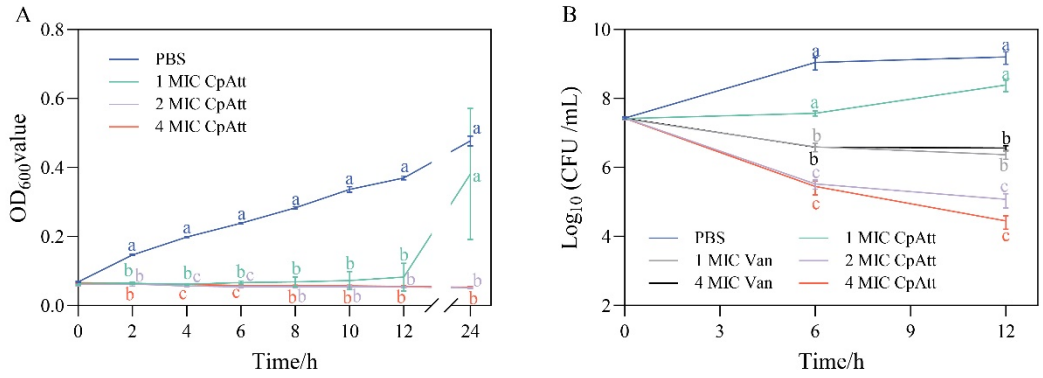


Fig. 1. Bacteriostatic curve (A) and time-killing curve (B) of *S. aureus* in response to CpAtt treatment. Data are presented as the mean ± standard deviation (n = 3). For a given time point, significant differences ($P < 0.05$) among treatment groups are indicated by different lowercase letters (a, b, c).

3.2 Effect of CpAtt on the ultrastructure of S. aureus

The effect of CpAtt on the ultrastructure of *S. aureus* was examined by TEM. In the control group, *S. aureus* cells exhibited a smooth and intact surface with no significant morphological alterations. In contrast, CpAtt-treated *S. aureus* displayed blurred cell wall and membrane structures, reduced intracellular electron density, and the formation of cavities (Fig. 2).

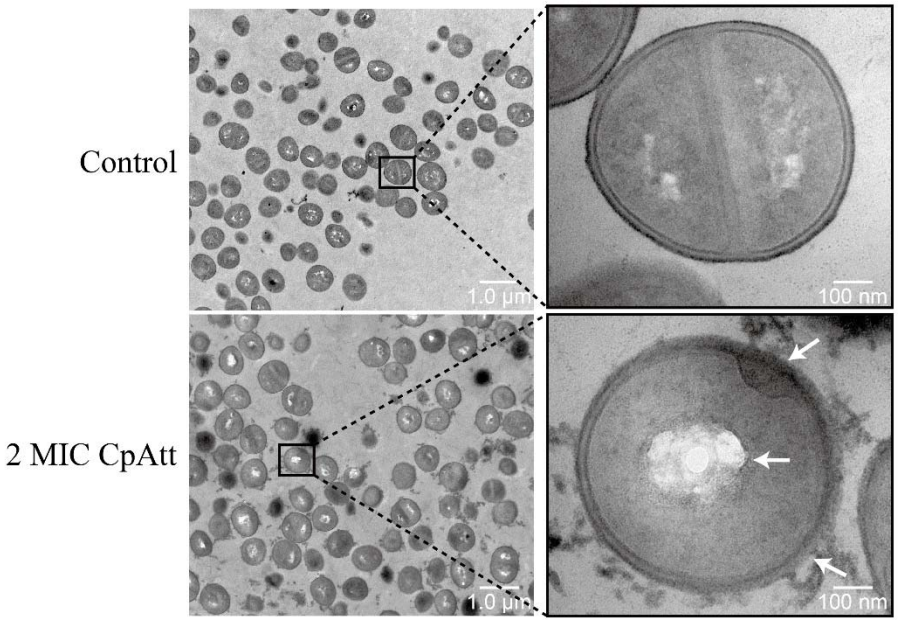


Fig. 2. Effect of CpAtt on the ultrastructure of *S. aureus*. White arrows indicate damaged regions.

3.3 Effect of CpAtt on the leakage of nucleic acids and proteins in S. aureus

The effect of CpAtt on the integrity of *S. aureus* was preliminarily evaluated by measuring the leakage of intracellular nucleic acids and proteins. As shown in Fig. 3, CpAtt significantly increased the leakage of intracellular nucleic acids and proteins in *S. aureus* in a dose-dependent and time-dependent manner compared to the control group.

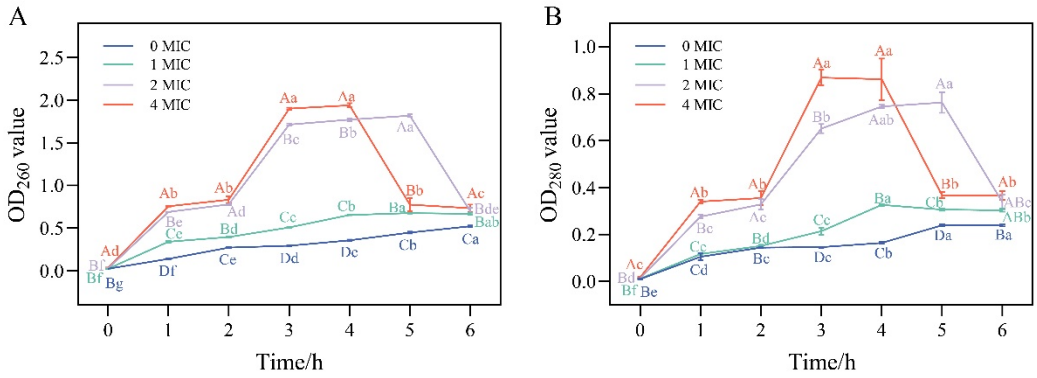


Fig. 3. Leakage of nucleic acids (A) and proteins (B) from *S. aureus* cells treated with CpAtt. Data are presented as the mean ± standard deviation (n = 3). At each time point, significant differences ($P < 0.05$) among treatment groups are indicated by different capital letters (A-D). Within the same treatment group, significant differences ($P < 0.05$) across time points are indicated by different lowercase letters (a-g).

3.4 Effect of CpAtt on the cell wall and membrane permeability in S. aureus

To assess the effect of CpAtt on the cell wall and membrane integrity of *S. aureus*, we further examined the leakage of intracellular ALP and β-galactosidase, as well as PI staining intensity. As shown in Fig. 4, CpAtt treatment significantly induced the leakage of ALP (Fig. 4A) and β-galactosidase (Fig. 4B) from *S. aureus* compared with the control group. Moreover, the fluorescence intensity of PI-stained *S. aureus* cells increased gradually with increasing CpAtt concentration (Fig. 4C).

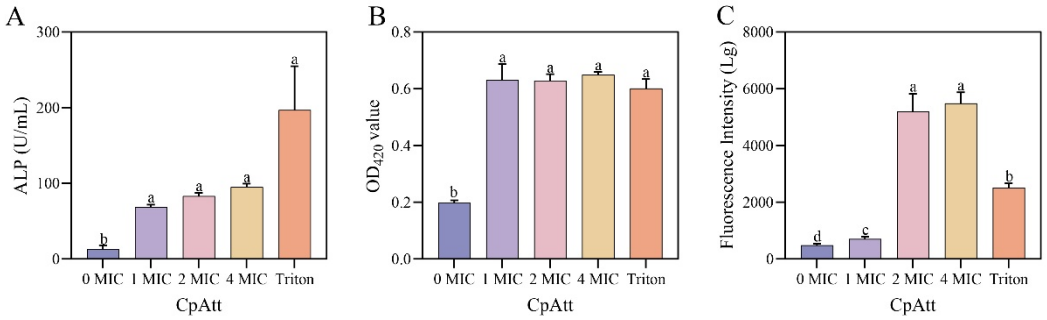
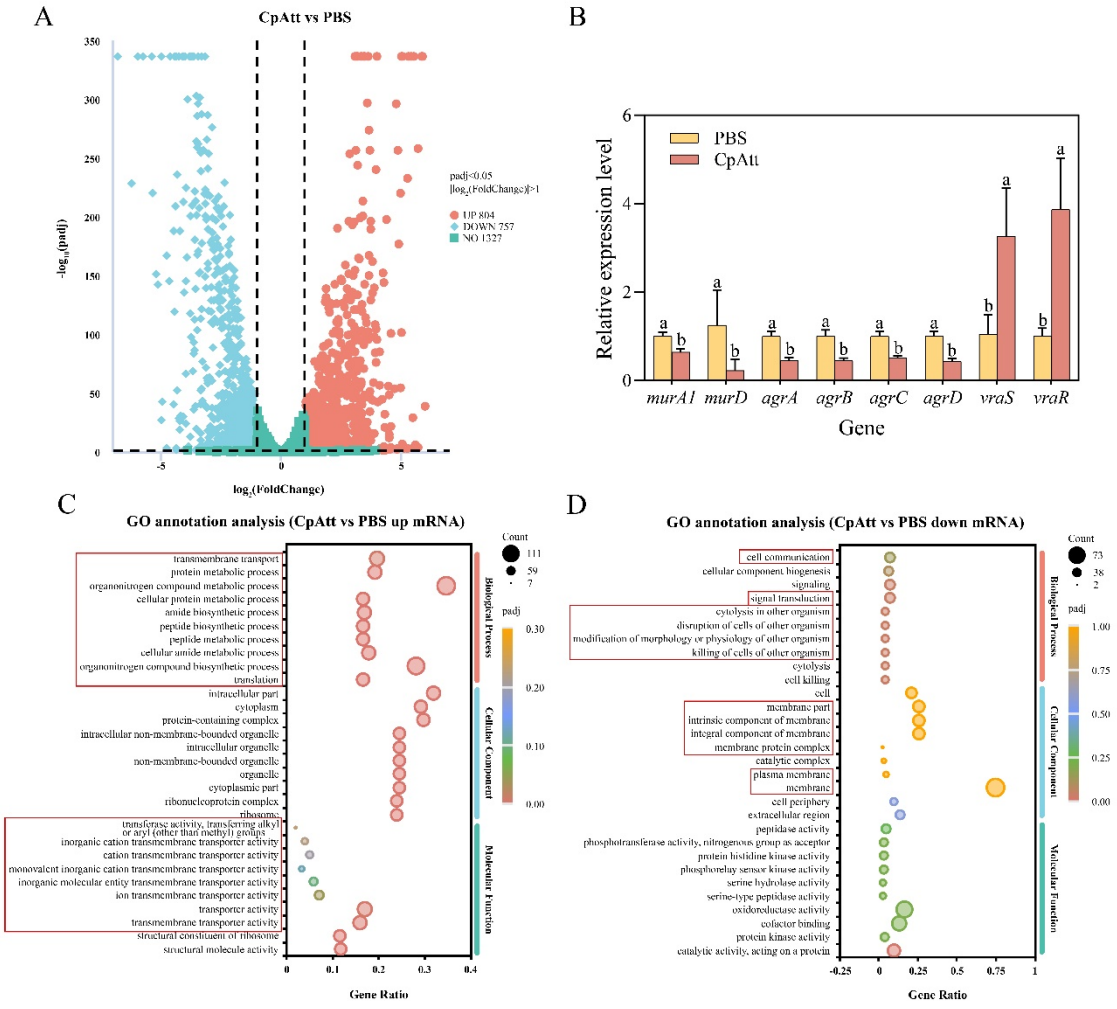


Fig. 4. Effect of CpAtt on the cell wall and membrane permeability of *S. aureus*. (A) Leakage of ALP. (B) Leakage of β-galactosidase. (C) Fluorescence intensity of PI staining. Data are presented as the mean ± standard deviation (n = 3). Significant differences ($P < 0.05$) among groups are indicated by different lowercase letters (a-d).

3.5 Quantitative and enrichment analysis of DEGs

To elucidate the antibacterial mechanism of CpAtt against *S. aureus*, we employed transcriptome sequencing to identify its potential antibacterial targets. The raw sequence data reported in this paper have been deposited in the Genome Sequence Archive of the National Genomics Data Center[35], China National Center for Bioinformation / Beijing Institute of Genomics, Chinese Academy of Sciences (GSA accession number: CRA036876), and are publicly accessible at https://ngdc.cncb.ac.cn/gsa. DEGs were identified using

DESeq2 software by comparative analysis between the CpAtt- and PBS-treated groups. Applying the threshold criteria of Padj < 0.05 and |log2 fold change| > 1, a total of 1561 DEGs were identified, of which 804 were upregulated and 757 were downregulated (Fig. 5A). To validate the RNA-Seq data, RT-qPCR was used to verify the transcription levels of selected DEGs. As shown in Fig. 5B, the results of RT-qPCR were consistent with those of RNA-Seq. We then conducted enrichment analysis of the upregulated and downregulated DEGs. According to GO annotation analysis, the upregulated DEGs were mainly enriched in biological processes related to the biosynthesis and metabolism of organonitrogen compounds, amide, peptide, and protein, as well as molecular functions of transport activity (Fig. 5C). The downregulated DEGs were mainly enriched in biological processes related with cell communication and the killing of other organisms. It is noteworthy that almost all downregulated DEGs were enriched in the membrane compartment (Fig. 5D). KEGG enrichment analysis further revealed that these upregulated DEGs were involved in various biosynthetic and metabolic pathways, as well as pathways related to β-lactam resistance (Fig. 5E). In contrast, downregulated DEGs were associated with pathways such as the citrate acid (TCA) cycle, nucleotide excision repair, the pentose phosphate pathway, and nucleotide sugar biosynthesis (Fig. 5F). Collectively, these results suggest that the antibacterial mechanism of CpAtt against *S. aureus* extends beyond membrane disruption and may also involve the disruption of intracellular metabolism, interference with transcription and translation machinery, and modulation of cell communication.



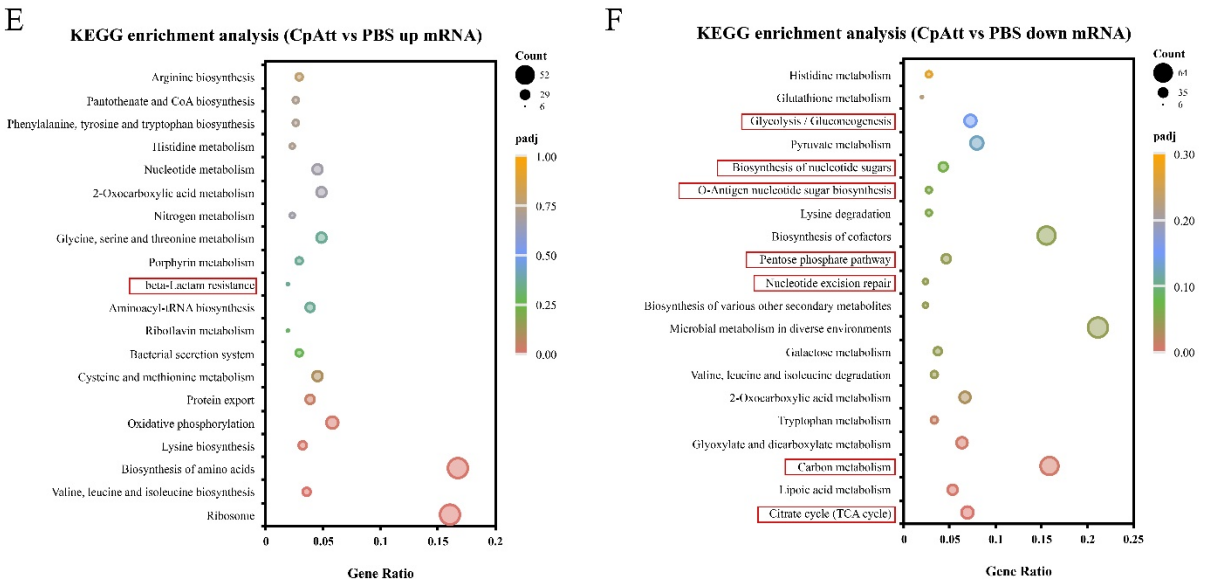


Fig. 5. Transcriptomic profile of *S. aureus* following CpAtt treatment. (A) Volcano plot of DEGs between control and CpAtt-treated groups. (B) RT-qPCR validation of the expression levels for eight selected DEGs. Data are presented as the mean ± standard deviation (n = 3). For each gene, significant differences ($P < 0.05$) between groups are indicated by different letters (a, b). (C and D) GO annotation of upregulated (C) and downregulated (D) DEGs. (E and F) KEGG pathway enrichment analysis of upregulated (E) and downregulated (F) DEGs.

3.6 Analysis of DEGs associated with cell wall biosynthesis

A detailed analysis of DEGs related to peptidoglycan synthesis revealed that *vraS* and *vraR*, belonging to the two-component system, were upregulated, while the peptidoglycan biosynthesis pathway was downregulated (Fig. 6). The results indicated that *S. aureus* underwent a stress response in its cell wall following CpAtt treatment, and this was accompanied by a reduction in peptidoglycan biosynthesis.

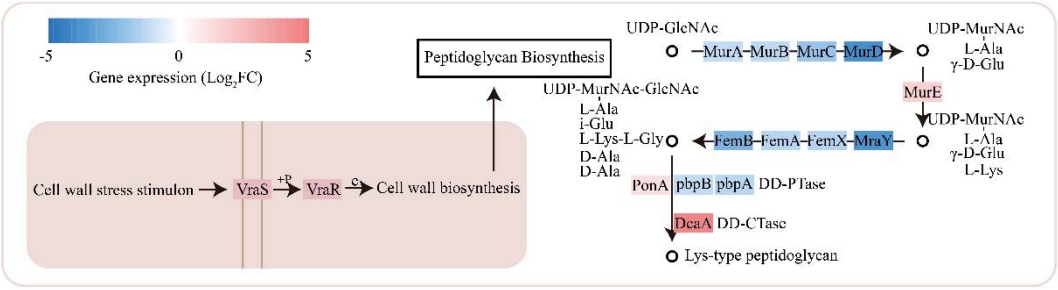


Fig. 6. Analysis of DEGs related to cell wall biosynthesis in *S. aureus.*

3.7 Effects of CpAtt on the intracellular metabolism of S. aureus

In the KEGG enrichment analysis, we observed that *S. aureus* underwent significant pathway enrichment related to energy metabolism and oxidative stress after CpAtt treatment (Fig. 5E, F). Subsequent in-depth analysis of the TCA cycle pathway and oxidative phosphorylation pathway revealed that compared with the control group, CpAtt-treated *S. aureus* downregulated the TCA cycle-related DEGs (Fig. 7A). For the oxidative phosphorylation pathway, CpAtt-treated *S. aureus* downregulated the DEGs associated with succinate dehydrogenase (SDH), and upregulated the DEGs related to F-type ATPase, Cytochrome c oxidase, and Cytochrome bd complex (Fig. 7B). ATP content measurement demonstrated a significant decrease in intracellular ATP levels of CpAtt-treated *S. aureus* (Fig. 7C). ROS content analysis revealed that compared with the control group, ROS accumulation did not increase but significantly decreased in the CpAtt-treated

groups (Fig. 7D). These results indicated that CpAtt disrupted *S. aureus* energy metabolism pathways, leading to intracellular ATP depletion, and did not cause ROS accumulation, differing from typical bactericidal antibiotics that induce oxidative stress.

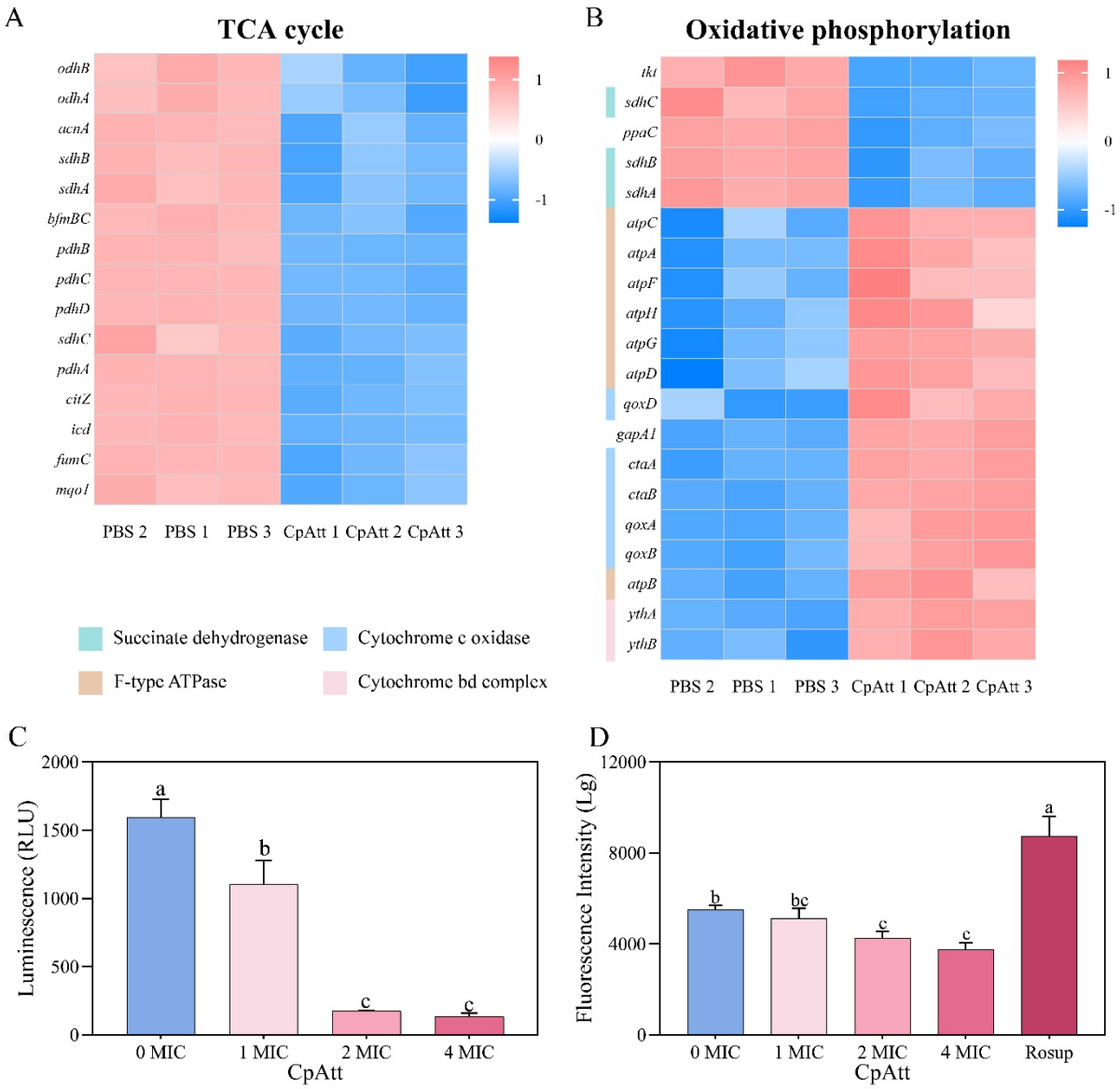


Fig. 7. Effects of CpAtt on the intracellular metabolism of *S. aureus*. (A and B) Heatmaps displaying the expression of DEGs associated with the TCA cycle (A) and oxidative phosphorylation (B). Corresponding gene names are listed on the left. (C and D) Intracellular levels of ATP (C) and ROS (D) in *S. aureus* treated with different concentrations of CpAtt. Data are presented as the mean ± standard deviation (n = 3). Significant differences ($P < 0.05$) among groups are indicated by different lowercase letters (a-c).

3.8 Analysis of CpAtt-S. aureus DNA interaction

Agarose gel electrophoresis was used to evaluate the interaction between CpAtt and *S. aureus* DNA. As shown in Fig. 8A, the DNA bands remained clear and bright in the untreated control, but gradually weakened with increasing CpAtt concentration. Notably, when the concentration ratio reached 5 and 10, the DNA bands exhibited significant smearing and blurring, while the brightness increased in the loading wells. Molecular docking was further employed to investigate the binding mode between CpAtt and DNA. The results revealed that CpAtt could bind to DNA (PDB ID: 2XCT) with a confidence score of 0.8692. According to Li et al.[36],

when the confidence score exceeds 0.7, the two molecules are highly likely to bind. Visualization of the model demonstrated that the positively charged end of the β-barrel structure formed hydrogen bonds with DNA (Fig. 8B). These findings suggested that CpAtt could interact with *S. aureus* DNA, potentially affecting intracellular DNA replication and translation processes.

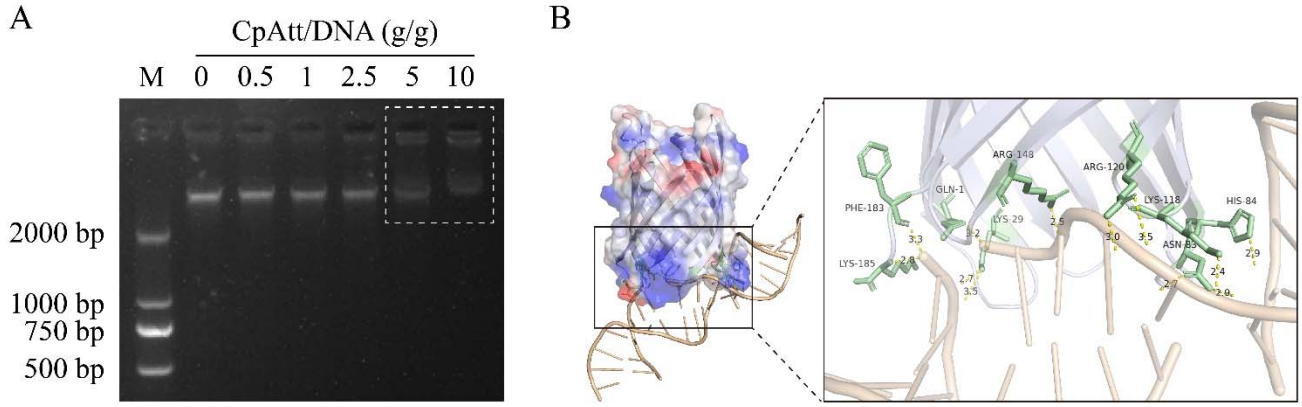


Fig. 8. Analysis of CpAtt-*S. aureus* DNA interaction. (A) Agarose gel electrophoresis of CpAtt with the genomic DNA of *S. aureus* in vitro. (B) Molecular docking pattern of CpAtt with *S. aureus* DNA, where blue indicates positive charges and red denotes negative charges.

3.9 Effect of CpAtt on the biofilm formation of S. aureus

RNA-seq analysis revealed that after CpAtt treatment, *agrA*, *agrB*, *agrC* and *agrD* were all downregulated in *S. aureus*. At the same time, *rot* was upregulated (Fig. 9A), indicating that the accessory gene regulator (agr) system of *S. aureus* was inhibited by CpAtt. Evaluation of *S. aureus* biofilm growth under sub-inhibitory concentrations of CpAtt showed that compared with the PBS group, 1/4 MIC CpAtt could prevent *S. aureus* from forming complete and dense biofilm, and under 1/2 MIC CpAtt, *S. aureus* almost failed to form biofilm with only partial bacterial adhesion (Fig. 9B). Quantitative detection after dissolving biofilm suggested that compared with the PBS group, biofilm formation of *S. aureus* was significantly reduced at concentrations of 1/4 MIC and 1/2 MIC (Fig. 9C). RT-qPCR analysis revealed that *icaA*, *icaB*, *icaD* were downregulated in *S. aureus* treated with sub-MIC CpAtt. In contrast to the inhibition of the agr system under high-concentration short-term treatment (1 MIC, 2 hours), *agrA* expression was upregulated following sub-inhibitory concentration long-term treatment (24 hours) (Fig. 9D). This upregulation may represent a compensatory response of bacteria after prolonged adaptation to low-dose stress. These results indicated that CpAtt affected the quorum sensing system of *S. aureus*, and under sub-MIC concentration, it regulated transcription of biofilm-related genes to inhibit biofilm formation.

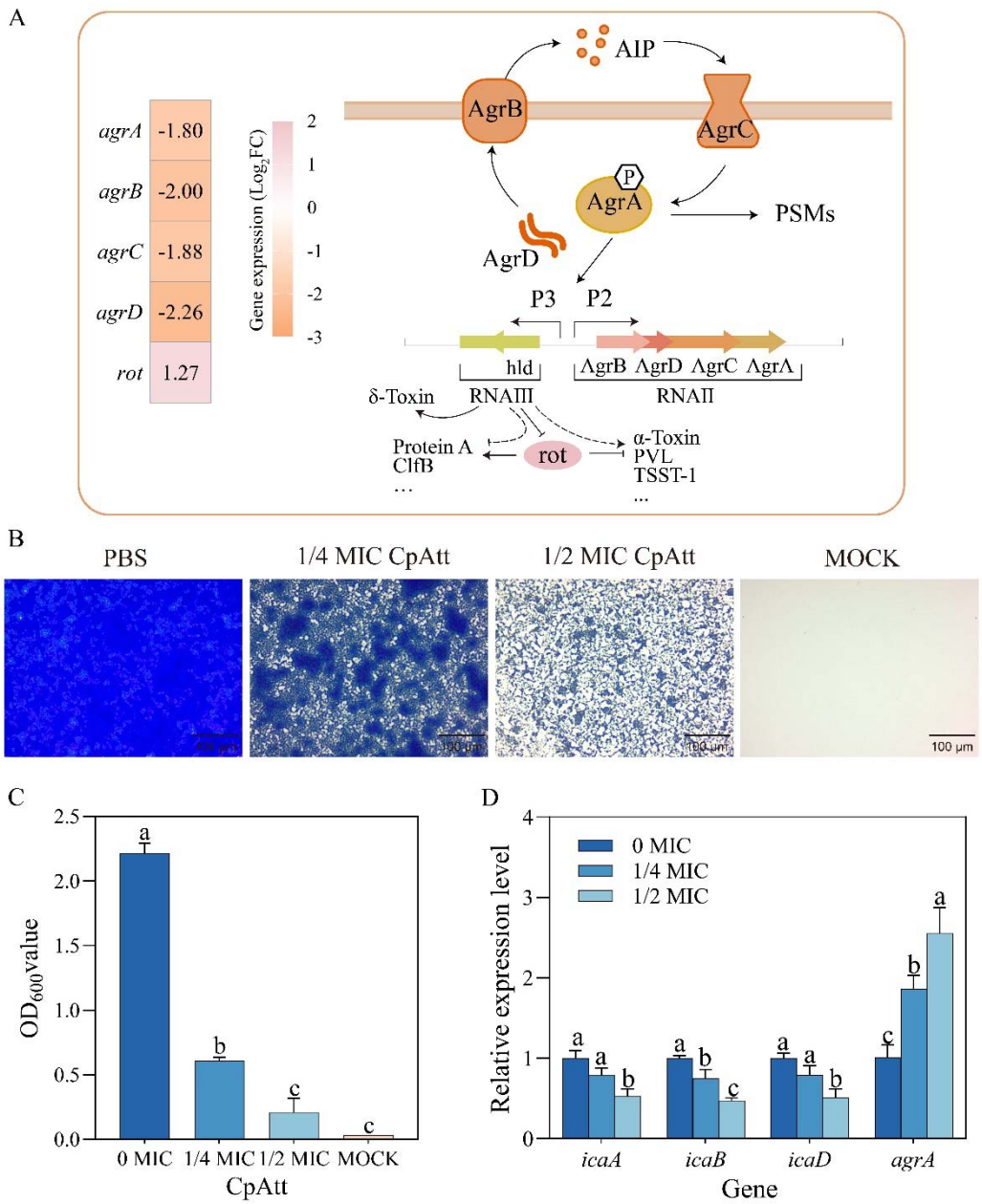


Fig. 9. Inhibitory effect of CpAtt on biofilm formation in *S. aureus*. (A) Schematic of the *S. aureus* agr quorum-sensing pathway. (B) Representative images of biofilms observed by inverted microscopy. (C) Quantitative analysis of biofilm biomass, determined by absorbance measurement. (D) RT-qPCR analysis of biofilm-related gene expression. Data are presented as the mean ± standard deviation (n = 3). Significant differences ($P < 0.05$) among groups are indicated by different lowercase letters (a-c).

3.10 CpAtt promoted the healing of skin wounds infected with S. aureus in mice

The *in vivo* efficacy of CpAtt against *S. aureus* was further assessed in a mouse skin wound infection model (Fig. 10A). As shown in Fig. 10B and 10C, compared with the negative control group, mice treated with CpAtt (10 μg) had better wound healing within 14 days after infection, which was similar to the blank control group. Surprisingly, CpAtt (20 μg) significantly reduced the amount of bacteria at the wound site in mice, but didn't promote wound healing, possibly due to its cytotoxic effect (Fig. 10D, E). Meanwhile, when compared with the negative control group, it was observed that CpAtt (10 μg) was able to reduce the bacterial load at the wound site by 35%. Consistently, histological analysis using H&E and Masson staining revealed a significant decrease in inflammatory cell infiltration and an increase in collagen deposition in wounds treated

with CpAtt (10 μg). These results collectively indicated that CpAtt promoted skin wound healing in mice infected with *S. aureus* when used at appropriate doses.

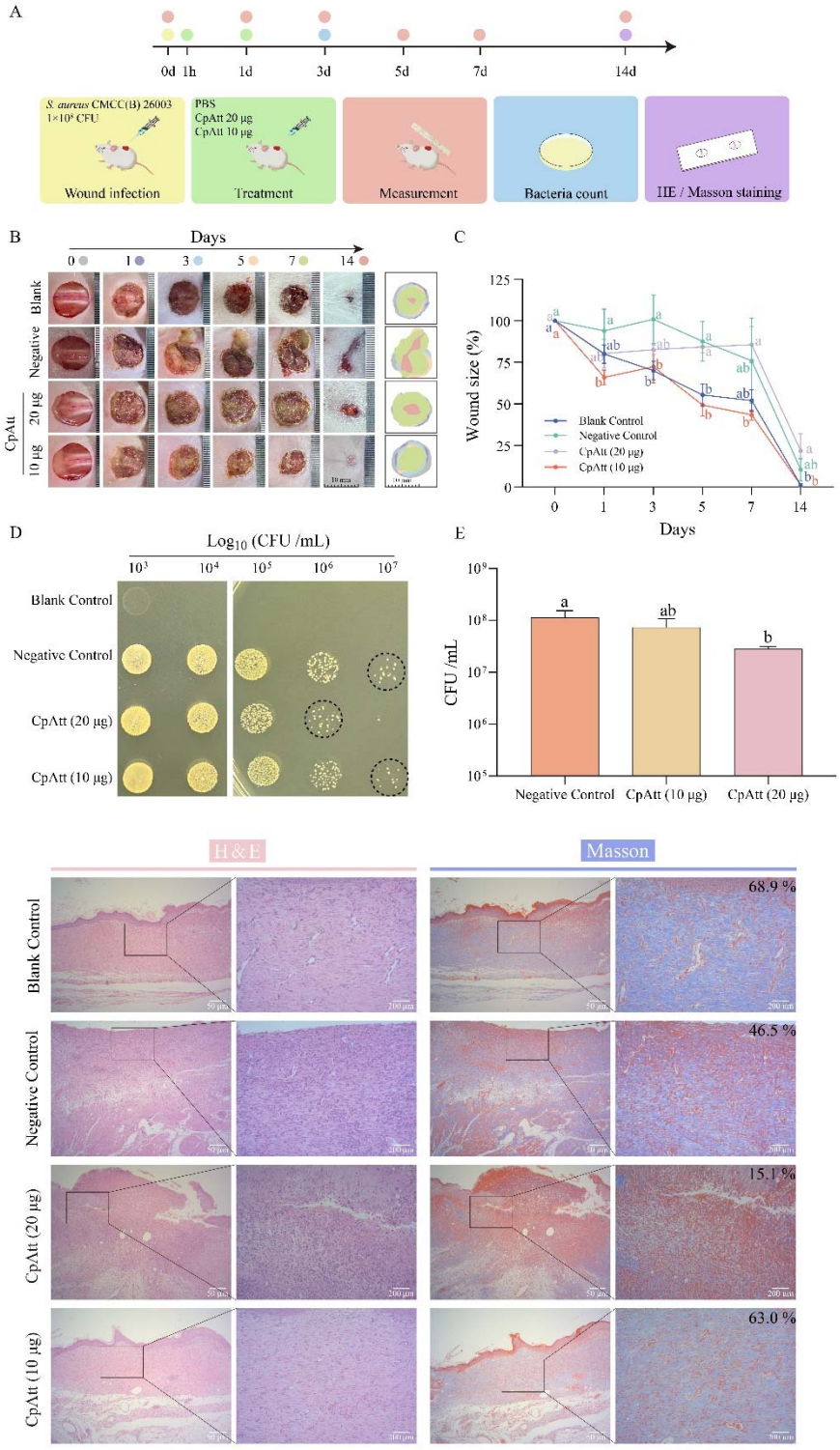


Fig. 10. Application of CpAtt in promoting healing of skin wounds infected with *S. aureus* in mice. (A) Timeline and procedure of the mouse skin wound infections model (n = 6 per group). (B) Representative photographs of different treatment groups. Photographs were taken on days 0, 1, 3, 5, 7, and 14 to record wound condition. (C) Percentage of wound size measured at the 1th, 3rd, 5th, 7th and 14th day. (D) and (E) Bacterial loads in wound tissues after drug treatments, determined by quantitative culturing on day 3 from infection sites. The detection limit of the experiment was 10^3 CFU/mL. All experiments were conducted with three biological replicates and data are presented as mean ± SD. Significant differences among groups were determined by ordinary one-way ANOVA ($P < 0.05$), with differences indicated by different lowercase letters (a, b). (F) H&E and Masson staining of the full-thickness skins. The collagen fiber percentage (from Masson staining) is shown in the upper right corner.

4. Discussion

Attacins are Gly-rich AMPs that exhibit inhibitory effects against both Gram-negative and Gram-positive bacteria [18, 21, 22]. Attacins employ multiple mechanisms to combat Gram-negative bacteria, including direct disruption of the bacterial outer membrane, interference with the synthesis of the bacterial outer membrane, and induction of intracellular stress protein production [18, 23, 24]. However, there are relatively few reports on the antimicrobial mechanisms of attacins against Gram-positive bacteria. This study focused on the antimicrobial mechanisms of CpAtt, an attacin AMP that exhibits antimicrobial activity against *S. aureus*[25].

CpAtt at a concentration of 37.5 μg/mL could significantly inhibit the growth of *S. aureus* within 12 hours (Fig. 1), while an attacin-like AMP, Hill_BB_C10074, did not inhibit the growth of *S. aureus*[24]. Subsequent TEM observations revealed that after treatment with CpAtt, the cell wall and membrane structures of *S. aureus* became indistinct, and the intracellular electron cloud density decreased (Fig. 2). Previous SEM studies had shown that CpAtt-treated *S. aureus* exhibited severe deformation and wrinkling[25]. It was reported by Xue et al.[37] that exposure to compound Gel@COF led to structural damage of the cell wall and a decrease in intracellular electron density in *S. aureus*, as revealed by SEM and TEM analysis. Therefore, it can be inferred that CpAtt could cause significant damage to both intracellular and extracellular structures of *S. aureus*. Furthermore, we observed significant leakage of intracellular components in *S. aureus* treated with CpAtt, including nucleic acids (Fig. 3A), proteins (Fig. 3B), ALP (Fig. 4A), and β-galactosidase (Fig. 4B). ALP is located between the cell membrane and cell wall, and β-galactosidase resides within the cell membrane. Therefore, these two indicators are usually used for evaluating cell wall and membrane permeability[27, 38]. Consequently, we proposed that CpAtt, like other AMPs such as Gloverin and Nisin, could damage the cell wall and membrane of *S. aureus* [27, 28]. This hypothesis was further validated by PI staining experiments (Fig. 4C).

The antimicrobial effects of AMPs typically damage bacterial membrane integrity, and can also exhibit multi-targeted antibacterial mechanisms such as disrupting energy metabolism, damaging bacterial DNA, and blocking bacterial quorum sensing[13, 30]. To elucidate the antibacterial mechanism of CpAtt against *S. aureus*, we employed transcriptomic sequencing to further analyze the potential antibacterial targets. Enrichment analysis of the selected DEGs revealed that genes related to biosynthesis and metabolism of amides, peptides, and proteins were upregulated (Fig. 5C, E), while pathways involving cell communication, bacterial killing capacity, energy metabolism, and nucleotide excision repair were downregulated (Fig. 5D, F). This pattern of transcriptional regulation closely resembled the effects of tannic acid on *S. aureus*, interestingly showing that tannic acid also compromised the integrity of *S. aureus* cell membranes[39].

It is well established that peptidoglycan is essential for *S. aureus* survival. Consequently, the enzymes and intermediate metabolites of its biosynthesis pathways represent prime targets for clinical antibiotics, exemplified by vancomycin and β-lactam antibiotics[40-41]. KEGG enrichment indicated an upregulation of β-lactamase resistance pathways. This finding suggested that CpAtt might compromise the cell wall and

membrane permeability of *S. aureus* via a mechanism analogous to that of β-lactam antibiotics, namely, the specific inhibition of peptidoglycan synthesis[42-43]. In this study, a cell wall stress response was observed. Concurrently, genes associated with peptidoglycan biosynthesis were downregulated (Fig. 6). The VraSR two-component system, comprising the histidine kinase VraS and the response regulator VraR, mediates the response of *S. aureus* to cell wall-targeting antibiotics, such as β-lactams and vancomycin[44-45]. These findings were consistent with the mode of action reported for other cell wall-targeting AMPs. For instance, transcriptomic analysis of *S. aureus* treated with the scorpion defensin BmKDfsin4 revealed downregulation of genes in the *mur* series (peptidoglycan synthesis) and *tag* series (lipoteichoic acid synthesis)[46]. Previous studies indicated that CpAtt demonstrated more potent antibacterial activity against Gram-positive bacteria,with a proposed mechanism involving binding to lipid II[25]. These results supported the hypothesis that the antibacterial action of CpAtt against *S. aureus* might involve targeting lipid II and/or key enzymes in peptidoglycan biosynthesis. However, the specific molecular interactions still need to be further elucidated.

Antibiotics usually do not rely solely on a single target, but on multiple targets to exert their antibacterial effects[15]. The bactericidal activity of some antibiotics was achieved through the perturbation of core metabolic processes such as the TCA cycle, which triggers a cascade that includes NADH depletion, iron-sulfur cluster destabilization, and Fenton reaction stimulation, culminating in hydroxyl radical-mediated oxidative damage[47]. The TCA cycle serves as the core pathway for aerobic oxidation, oxidizing acetyl-CoA to generate high-energy molecules and providing reducing equivalents to the electron transport chain (ETC)[48]. Under antibiotic pressure, bacteria universally adopt a "low metabolism" or dormancy state, a strategy that involves the downregulation of central carbon metabolism to reduce the cellular energy burden and promote survival[49-50]. Consistent with this paradigm, genes associated with the TCA cycle were downregulated in *S. aureus* under CpAtt stress (Fig. 7A), indicating a shift to a low-metabolism mode. Notably, the transcription of SDH, a key TCA cycle enzyme that also directly feeds electrons into the respiratory chain, showed a further reduction. This decrease would be expected to further diminish TCA flux[50]. However, in the context of compromised cell membrane integrity, inhibition of the TCA cycle inevitably reduces the efficiency of the ETC[51]. The F-type ATPase typically relies on the proton motive force (PMF) to synthesize ATP. However, upon dissipation of the transmembrane PMF or a decrease in membrane potential, the ATPase reverses its function, hydrolyzing ATP to pump protons outward in an attempt to maintain membrane potential[52-53]. The intracellular ATP content of *S. aureus* was measured following CpAtt treatment. As expected, a significant decrease in ATP levels was observed (Fig. 7C). It is hypothesized that this reduction was collectively due to inhibition of the TCA cycle and the consumption of ATP by F-type ATPase to maintain membrane potential. Although the potential contribution of ATP leakage through the compromised membrane cannot be excluded[49, 54].These findings reflect a low-metabolic stress state adopted by bacteria upon encountering membrane structural damage. Although bacteria attempt to reduce central carbon metabolism flux to alleviate the energy burden, this compensatory mechanism fails to prevent ATP depletion once membrane integrity is compromised.

Within the oxidative phosphorylation pathway, the upregulation of DEGs related to cytochrome c oxidase and cytochrome bd complex reflected an adaptive response aimed at alleviating oxidative stress. Cytochrome c oxidase catalyzes the final electron transfer to molecular oxygen and is associated with lower ROS production Concurrently, induction of the cytochrome bd complex, a well-characterized stress-adaptive terminal oxidase under challenges like antibiotic exposure or hypoxia, further contributes to ROS minimization and promotes survival[55-56]. ROS is an inevitable byproduct of aerobic metabolism, when accumulated to excessive levels, ROS could result in bacterial metabolic disruption, protein misfolding, DNA damage, and ultimately cell death[57]. Consequently, the targeted induction of high intracellular ROS concentrations is regarded as a common mechanistic strategy for numerous antimicrobial agents[15, 58, 59]. In contrast to typical bactericidal antibiotics, CpAtt treatment did not elevate intracellular ROS in *S. aureus* but caused a significant reduction at 2 MIC (Fig. 7D), indicating a non-canonical mechanism distinct from ROS-mediated bactericidal activity. Inhibition of the TCA cycle reduced electron flux into the chain, limiting ROS generation, while induction of the oxidases promoted ROS detoxification. Collectively, these adaptations resulted in a net decrease in cellular ROS. However, the above inference has not yet been directly verified at the protein or enzyme activity level, which represents a major limitation of this study. In future research, we will use enzyme activity assay kits to measure changes in the activities of key TCA cycle enzymes and assess the expression levels of oxidative phosphorylation-related proteins via Western blotting.

As the core of bacterial life activities, DNA is essential for genetic information storage and physiological regulation[60]. Treated DNA displayed marked smearing and aberrant migration on agarose gels, along with the signal intensity an increase in the wells (Fig. 8A), a pattern consistent with compound-induced binding and aggregation[33]. Molecular docking predicted that this binding was driven by the non-specific electrostatic interactions, whereby basic residues (e.g., LYS, HIS, ARG) on CpAtt engage the negatively charged DNA backbone[61-62]. These results demonstrated the *in vitro* binding potential between CpAtt and *S. aureus* DNA. We hypothesize that membrane disruption is a prerequisite for DNA binding. In intact bacteria, large molecules cannot readily cross the intact cell membrane to enter the cytoplasm. Thus, binding of CpAtt to DNA likely occurs only after membrane disruption. In other words, increased membrane permeability enables CpAtt to enter the cell and access DNA. However, the above model represents a rational speculation based on currently available data and is subject to certain limitations. Specifically, we did not examine DNA replication-related gene expression, DNA synthesis rate, or protein synthesis levels. Consequently, the impact of CpAtt-DNA binding on the bacterial central dogma remains speculative and requires direct validation in future studies. Moreover, the agarose gel retardation assay did not include calf thymus DNA as a negative control, so non-specific binding of CpAtt to DNA cannot be excluded. In addition, no in vitro pull-down assays were performed to experimentally verify the actual binding between CpAtt and DNA. Therefore, the current binding results are largely predictive and warrant further validation using more rigorous biophysical methods.

The agr system is a key determinant of *S. aureus* virulence, therefore the inhibition of its effectors is considered a promising strategy for mitigating infection[63-64]. The Agr system exerts regulation primarily through AgrA-dependent transcription of RNAIII from the P3 promoter. RNAIII serves as both an mRNA encoding δ-toxin and a multifunctional regulatory factor that binds to target mRNAs to exert its functions[64]. Its regulatory activity includes the translational repression of Rot, a master transcriptional repressor of genes for lipases, hemolysins, proteases, and other secreted proteins. RNAIII inhibits Rot to thereby derepress these virulence gene transcription[65]. Transcriptional analysis revealed that CpAtt induced downregulation of the agr locus genes (*agrA-D*) and an antagonistic upregulation of the regulator rot (Fig. 9A). These findings demonstrated that CpAtt inhibited the agr system, resulting in disruption of *S. aureus* quorum sensing. Biofilm formation is the structured bacterial community encased in an extracellular polymeric matrix and makes bacteria readily adhere to surfaces, which leads to persistent contamination and enhances antibiotic resistance[8, 9, 66]. At sub-inhibitory concentrations, CpAtt impeded the development of intact biofilms in *S. aureus* (Fig. 9B, C). The discrepancy in *agrA* expression between Fig. 9A and 9D arises from the different experimental conditions. Under long-term sub-inhibitory concentration treatment, *agrA* expression was upregulated, which aligns with the known regulation of the Agr system by fosfomycin[67]. Consistent with this phenotype, transcriptional analysis after 24 h growth under sub-MIC CpAtt revealed downregulation of the *icaA*, *icaB*, and *icaD* genes, alongside an upregulation of agrA (Fig. 9D). In *S. aureus*, the *ica* operon genes mediate the production of polysaccharide intercellular adhesion (PIA), a key determinant of biofilm formation[68, 69]. However, the Agr system promotes biofilm dispersal by regulating RNAIII transcription and repressing adhesion protein expression[69-71]. Therefore, it was concluded that CpAtt disrupted the quorum-sensing system and mediated PIA production and adhesion protein expression, thereby affecting biofilm formation in *S. aureus*[72]. Nevertheless, this study did not investigate quorum-sensing signal molecule concentrations or the potential direct interaction of CpAtt with AgrC/AgrA. Consequently, the upstream regulatory mechanism remains undefined, representing a major limitation of this work.

Using a mouse skin infection model, we found that two doses of CpAtt treatment effectively reduced the bacterial load around the wound and promoted healing. We attribute the difference in bacterial load measured on day 3 primarily to the cumulative antibacterial effect of the two administrations rather than the sustained effect of a single dose, given that 48 hours had elapsed since the last administration by day 3. For antimicrobial peptides such as CpAtt, the effective concentration in the wound environment is typically maintained for a limited duration. The two administrations covered the critical 0-24 hour window post-infection, providing continuous bacterial growth inhibition and leading to a detectable difference in bacterial load on day 3. However, the absence of a single-administration control group precludes a strict distinction between whether the day-3 effect is entirely due to the cumulative effect of two doses or whether the first dose already produced the primary effect and the second only maintained or enhanced it. Nonetheless, this limitation does not affect the overall conclusion that CpAtt treatment effectively reduces the bacterial load around mouse wounds. The accelerated wound closure and histological improvement observed on day 14 are primarily a secondary

consequence of the reduced bacterial load achieved in the early stage. The two initial administrations effectively lowered the bacterial burden at the wound site, thereby creating favorable conditions for the host's intrinsic repair mechanisms, including alleviation of persistent inflammatory damage, promotion of collagen deposition, and acceleration of re-epithelialization. In other words, the early antibacterial effect appears sufficient to trigger a cascade of healing processes that continue beyond the period of drug presence[15].

In summary, we demonstrated that CpAtt is a multi-target peptide belonging to the attacin family. To clarify the antibacterial mechanism of attacin against Gram-positive bacteria, the antibacterial mechanism of CpAtt against *S. aureus* was elucidated, and the effect of CpAtt on *S. aureus* infection *in vivo* was preliminarily evaluated. Unlike traditional antibacterial agents that act on a single target, the antibacterial mechanism of the cationic antimicrobial peptide CpAtt is rooted in its intrinsic physicochemical properties. These features enable CpAtt to bind simultaneously to multiple negatively charged targets on the bacterial surface through electrostatic interactions, thereby disrupting cell membrane integrity. It can further penetrate into the cell interior to interfere with energy metabolism and DNA functions. This multi-level, multi-target mode of action fundamentally differs from that of conventional single-target drugs and is expected to reduce the risk of bacterial resistance[10, 72]. Nevertheless, there are some limitations in this study, such as the specific molecular mechanism by which CpAtt inhibits peptidoglycan biosynthesis remains unclear. Furthermore, CpAtt was applied to the skin wounds infected with *S. aureus* in mice, the higher dose more effectively eliminated bacteria at the wound, but its ability to promote wound healing was not as good as that of the lower dose, which may be due to the cytotoxicity of higher doses.Future clinical studies should determine the median lethal dose and maximum tolerated dose of CpAtt and compare its efficacy with that of currently used clinical antibacterial agents. Moreover, modification of natural CpAtt to improve its activity and safety, together with the development of safer and more efficient expression systems, would facilitate its production and clinical application.

5. Conclusions

This study elucidated the antibacterial mechanisms of the peptide CpAtt against *S. aureus*. CpAtt primarily targeted the cell wall and membrane, causing structural disruption and consequent leakage of intracellular components. Furthermore, it interfered with critical physiological processes, including the inhibition of peptidoglycan synthesis, perturbation of intracellular metabolism, and non-specific binding to genomic DNA. Additionally, CpAtt modulated the transcription of adhesion-related genes, thereby impeding biofilm formation. Consistently, *in vivo* experiments demonstrated that CpAtt promoted skin wound healing in mice while protecting against infection when administered at appropriate doses. Therefore, this work provides insight into the antibacterial mechanism of attacin against Gram-positive bacteria and offers a basis for the development of green biological control agents targeting Gram-positive bacteria.

Conflict of interest

The authors have no conflicts of interest to declare.

Acknowledgment

This research was sponsored by Science and Technology Research Project of Henan Province (262102110014), Hebei Provincial Modern Agro-industry Technology System of China (HBCT2024220208), Doctoral Research Fund for Anyang Institute of Technology (BSJ2024005).

Data availability

Data will be made available on request.

References

Z.T. Rani, L.C. Mhlongo, A. Hugo, Microbial profiles of meat at different stages of the distribution chain from the abattoir to retail outlets, Int. J. Environ. Res. Public Health 20(3) (2023) 1986. https://doi.org/10.3390/ijerph20031986.

J.A. Kluytmans, H.F. Wertheim, Nasal carriage of *Staphylococcus aureus* and prevention of nosocomial infections, Infection 33(1) (2005) 3-8. https://doi.org/10.1007/s15010-005-4012-9.

S.Y. Tong, J.S. Davis, E. Eichenberger, et al., *Staphylococcus aureus* infections: epidemiology, pathophysiology, clinical manifestations, and management, Clin. Microbiol. Rev. 28(3) (2015) 603-6619. https://doi.org/10.1128/CMR.00134-14.

Y. Mikhaylova, A. Shelenkov, A. Chernyshkov, et al., Whole-genome analysis of *Staphylococcus aureus* isolates from ready-to-eat food in russia, Foods 11(17) (2022) 2574. https://doi.org/10.3390/foods11172574.

A.R. Tomé, F.M. Carvalho, R. Teixeira-Santos, et al., Use of probiotics to control biofilm formation in food industries, Antibiotics (Basel) 12(4) (2023) 754. https://doi.org/10.3390/antibiotics12040754.

Z. Zhao, X. Wei, A. Wang, et al., A foodborne outbreak associated with ST59-spa t441-SCCmec IVa methicillin-resistant *Staphylococcus aureus* producing enterotoxins A and B - Puyang city, Henan province, China, September 2024, China CDC. Wkly 7(33) (2025) 1093-1098. https://doi.org/10.46234/ccdcw2025.184.

Antimicrobial Resistance Collaborators. Global burden of bacterial antimicrobial resistance in 2019: a systematic analysis, Lancet 399(10325) (2022) 629-655. https://doi.org/10.1016/S0140-6736(21)02724-0.

W. Hou, S. Kang, J. Chang, et al., Correlation analysis between GlpQ-regulated degradation of wall teichoic acid and biofilm formation triggered by lactobionic acid in *Staphylococcus aureus*, Foods 11(21) (2022) 3438. https://doi.org/10.3390/foods11213438.

H. Guo, Y. Tong, J. Cheng, et al., Biofilm and small colony variants-an update on *Staphylococcus aureus* strategies toward drug resistance, Int. J. Mol. Sci. 23(3) (2022) 1241. https://doi.org/10.3390/ijms23031241.

N. Yang, D. Wang, F. Yu, et al., Harnessing innovations in antimicrobial peptide design: From AI-driven discovery to precision targeting mechanisms, Food & Medicine Homology. 2(3) (2025) 9420121. https://doi.org/10.26599/FMH.2025.9420121

K. Xu, X. Zhao, Y. Tan, et al., A systematical review on antimicrobial peptides and their food applications, Biomater. Adv. 155 (2023) 213684. https://doi.org/10.1016/j.bioadv.2023.213684.

G. Wang, C. Schmidt, X. Li, et al., APD6: the antimicrobial peptide database is expanded to promote research and development by deploying an unprecedented information pipeline, Nucleic Acids Res. 54(D1) (2026) D363-D374. https://doi.org/10.1093/nar/gkaf860.

N.G. Oliveira Júnior, C.M. Souza, D.F. Buccini, et al., Antimicrobial peptides: structure, functions and translational applications, Nat. Rev. Microbiol. 23 (2025) 687–700. https://doi.org/10.1038/s41579-025-01200-y.

T. Schneider, T. Kruse, R. Wimmer, et al., Plectasin, a fungal defensin, targets the bacterial cell wall precursor Lipid II, Science 328(5982) (2010) 1168-1172. https://doi.org/10.1126/science.1185723.

J. Shi, C. Chen, P. Kong, et al., Non-Membrane active peptide resensitizes MRSA to β-Lactam antibiotics and inhibits *S. aureus* virulence, Adv. Sci. (Weinh). 12(15) (2025) e2416260. https://doi.org/10.1002/advs.202416260.

T. Sneideris, N.A. Erkamp, H. Ausserwöger, et al., Targeting nucleic acid phase transitions as a mechanism of action for antimicrobial peptides, Nat. Commun. 14(1) (2023) 7170. https://doi.org/10.1038/s41467-023-42374-4.

F. Buonocore, A.M. Fausto, G. Della Pelle, et al., Attacins: A promising class of insect antimicrobial peptides, Antibiotics (Basel) 10(2) (2021) 212. https://doi.org/10.3390/antibiotics10020212.

P. Engström, A. Carlsson, A. Engström, et al., The antibacterial effect of attacins from the silk moth *Hyalophora cecropia* is directed against the outer membrane of Escherichia coli, EMBO J. 3(13) (1984) 3347-3351. https://doi.org/10.1002/j.1460-2075.1984.tb02302.x.

D. Hultmark, A. Engström, K. Andersson, et al., Insect immunity. Attacins, a family of antibacterial proteins from *Hyalophora cecropia*, EMBO J. 2(4) (1983) 571-576. https://doi.org/10.1002/j.1460-2075.1983.tb01465.x.

A. Carlsson, P. Engström, E.T. Palva, et al., Attacin, an antibacterial protein from *Hyalophora cecropia*, inhibits synthesis of outer membrane proteins in *Escherichia coli* by interfering with omp gene transcription, Infect. Immun. 59(9) (1991) 3040-3045. https://doi.org/10.1128/iai.59.9.3040-3045.1991.

K. Bang, S. Park, J.Y. Yoo, et al., Characterization and expression of attacin, an antibacterial protein-encoding gene, from the beet armyworm, Spodoptera exigua (Hübner) (Insecta: Lepidoptera: Noctuidae), Mol. Biol. Rep. 39(5) (2012) 5151-5159. https://doi.org/10.1007/s11033-011-1311-3.

H.S. Shin, S.I. Park, Novel attacin from Hermetia illucens: cDNA cloning, characterization, and antibacterial properties, Prep. Biochem. Biotechnol. 49(3) (2019) 279-285. https://doi.org/10.1080/10826068.2018.1541807.

A. Carlsson, T. Nyström, H. de Cock, et al., Attacin-an insect immune protein-binds LPS and triggers the specific inhibition of bacterial outer-membrane protein synthesis, Microbiology (Reading) 144 (Pt 8) (1998) 2179-2188. https://doi.org/10.1099/00221287-144-8-2179.

L. Fahmy, Y.M. Ali, D. Seilly, et al., An attacin antimicrobial peptide, Hill_BB_C10074, from *Hermetia illucens* with anti-*Pseudomonas aeruginosa* activity, BMC Microbiol. 23(1) (2023) 378. https://doi.org/10.1186/s12866-023-03131-1.

Y. Wang, L. Zhou, Q. Feng, et al., Identification and antibacterial activity of a novel antimicrobial peptide attacin from *Conogethes punctiferalis*, Arch. Microbiol. 207(9) (2025） 223. https://doi.org/10.1007/s00203-025-04432-x.

L. Zhou, K. Lian, M. Wang, et al., The antimicrobial effect of a novel peptide LL-1 on *Escherichia coli* by increasing membrane permeability, BMC Microbiol. 22(1) (2022) 220. https://doi.org/10.1186/s12866-022-02621-y.

J. Guo, Y. Liu, L. Wei, et al., Insight into the synergistic antibacterial effect of Nisin and Chinese chive seed extract against *Staphylococcus aureus* and their application in pasteurized milk, Food Microbiol. 131 (2025) 104816. https://doi.org/10.1016/j.fm.2025.104816.

K. Lian, Y. Wang, Y. Jiao, et al., Identification and expression of a novel antimicrobial peptide Gloverin and its antibacterial effect against *Staphylococcus aureus*, BMC Microbiol. 25(1) (2025) 554. https://doi.org/10.1186/s12866-025-04197-9.

J. Feng, Y. Zheng, W. Ma, et al., A synthetic antibiotic class with a deeply-optimized design for overcoming bacterial resistance, Nat. Commun. 15(1) (2024) 6040. https://doi.org/10.1038/s41467-024-50453-3.

Y. Li, S. Li, K. Yang, et al., Antibiofilm mechanism of a novel milk-derived antimicrobial peptide against Staphylococcus aureus by downregulating agr quorum sensing system, J. Appl. Microbiol. 133(4) (2022) 2198-2209. https://doi.org/10.1111/jam.15653.

T. Yi, Y. Huang, Y. Chen, Production of an antimicrobial peptide AN5-1 in *Escherichia coli* and its dual mechanisms against bacteria, Chem. Biol. Drug Des. 85(5) (2015) 598-607. https://doi.org/10.1111/cbdd.12449.

Y. Yan, S.Y. Huang, Modeling protein-protein or protein-DNA/RNA complexes using the HDOCK webserver, Methods Mol. Biol. 2165 (2020) 217-229. https://doi.org/10.1007/978-1-0716-0708-4_12.

W. Tao, W. Li, J.J. Aweya, et al., Bacillus subtilis fermented shrimp waste isolated peptide, PVQ9, and its antimicrobial mechanism on four Gram-positive foodborne bacteria, Food Microbiol. 125 (2025) 104654. https://doi.org/10.1016/j.fm.2024.104654.

D. Fang, T. Xu, F. Li, et al., Methionine-driven methylation modification overcomes plasmid-mediated high-level tigecycline resistance, Nat. Commun. 16(1) (2025) 417. https://doi.org/10.1038/s41467-024-55791-w.

CNCB-NGDC Members and Partners. Database resources of the National Genomics Data Center, China National Center for bioinformation in 2024, Nucleic Acids Res. 52(D1) (2024) D18-D32. https://doi.org/10.1093/nar/gkad1078.

H. Li, E. Huang, Y. Zhang, et al., HDOCK update for modeling protein-RNA/DNA complex structures, Protein Sci. 31(11) (2022) e4441. https://doi.org/10.1002/pro.4441.

Y. Xue, X. Chen, F. Wu, et al., A self-oxidizing O-dihydroxybenzene-based covalent organic framework hydrogel with broad-spectrum antibacterial properties for promoting diabetic wound healing, Adv. Funct. Mater. 35 (2025) 2505669. https://doi.org/10.1002/adfm.202505669.

Z. Wang, Q. Yang, X. Wang, et al., Antibacterial activity of xanthan-oligosaccharide against *Staphylococcus aureus* via targeting biofilm and cell membrane, Int. J. Biol. Macromol. 15 (2020) 153:539-544. https://doi.org/10.1016/j.ijbiomac.2020.03.044.

J. Wang, Z. Sheng, Y. Liu, et al., Combined proteomic and transcriptomic analysis of the antimicrobial mechanism of tannic acid against *Staphylococcus aureus*, Front. Pharmacol. 14 (2023) 1178177. https://doi.org/10.3389/fphar.2023.1178177.

D. Gutiérrez, L. Fernández, A. Rodríguez, et al., Are phage lytic proteins the secret weapon to kill *Staphylococcus aureus*?, mBio. 9(1) (2018) e01923-17. https://doi.org/10.1128/mBio.01923-17.

X. Hua, Y. Jia, Q. Yang, et al., Transcriptional analysis of the effects of gambogic acid and neogambogic acid on methicillin-resistant *Staphylococcus aureus*, Front. Pharmacol. 10 (2019) 986. https://doi.org/10.3389/fphar.2019.00986.

D.J. Tipper, J.L. Strominger, Mechanism of action of penicillins: a proposal based on their structural similarity to acyl-D-alanyl-D-alanine, Proc. Natl. Acad. Sci. U. S. A. 54(4) (1965) 1133-41. https://doi.org/10.1073/pnas.54.4.1133.

H. Cho, T. Uehara, T.G. Bernhardt, Beta-lactam antibiotics induce a lethal malfunctioning of the bacterial cell wall synthesis machinery, Cell 159(6) (2014) 1300-11. https://doi.org/10.1016/j.cell.2014.11.017.

S. Gardete, S.W. Wu, S. Gill, et al., Role of VraSR in antibiotic resistance and antibiotic-induced stress response in Staphylococcus aureus, Antimicrob. Agents Chemother. 50(10) (2006) 3424-34. https://doi.org/10.1128/AAC.00356-06.

M. Germain, H. Robin, K.B. Le Huyen, et al., sRNA-mediated crosstalk between cell wall stress and galactose metabolism in *Staphylococcus aureus*, Nucleic Acids Res. 53(13) (2025) gkaf616. https://doi.org/10.1093/nar/gkaf616.

X. Yang, H. Zhang, S. Lu, et al., Insights into the antimicrobial mechanisms of a scorpion defensin on *Staphylococcus aureus* using transcriptomic and proteomic analyses, Molecules 30(7) (2025) 1542. https://doi.org/10.3390/molecules30071542.

M.A. Kohanski, D.J. Dwyer, B. Hayete, et al., A common mechanism of cellular death induced by bactericidal antibiotics, Cell 130(5) (2007) 797-810. https://doi.org/10.1016/j.cell.2007.06.049.

L. Guo, F-ATP synthase inhibitory factor 1 and mitochondria-organelle interactions: New insight and implications, Pharmacol. Res. 208 (2024) 107393. https://doi.org/10.1016/j.phrs.2024.107393.

E.A. Zalis, A.S. Nuxoll, S. Manuse, et al., Stochastic variation in expression of the tricarboxylic acid cycle produces persister cells, mBio. 10(5) (2019) e01930-19. https://doi.org/10.1128/mBio.01930-19.

J. Chen, C. Tang, R. Zhang, et al., Metabolomics analysis to evaluate the antibacterial activity of the essential oil from the leaves of *Cinnamomum camphora* (Linn.) Presl, J. Ethnopharmacol. 253 (2020) 112652. https://doi.org/10.1016/j.jep.2020.112652.

H. Niu, J. Gu, Y. Zhang, Bacterial persisters: molecular mechanisms and therapeutic development, Signal Transduct. Target. Ther. 9(1) (2024) 174. https://doi.org/10.1038/s41392-024-01866-5.

T.L. To, J.G. McCoy, N.K. Ostriker, et al., PMF-seq: a highly scalable screening strategy for linking genetics to mitochondrial bioenergetics, Nat. Metab. 6(4) (2024) 687-696. https://doi.org/10.1038/s42255-024-00994-0.

W. Kühlbrandt, Structure and mechanisms of F-Type ATP synthases, Annu. Rev. Biochem. 88 (2019) 515-549. https://doi.org/10.1146/annurev-biochem-013118-110903.

G. Akanuma, T. Tagana, M. Sawada, et al., C-terminal regulatory domain of the ε subunit of Fo F1 ATP synthase enhances the ATP-dependent H+ pumping that is involved in the maintenance of cellular membrane potential in Bacillus subtilis, Microbiologyopen 8(8) (2019) e00815. https://doi.org/10.1002/mbo3.815.

P. Lu, M.H. Heineke, A. Koul, et al., The cytochrome bd-type quinol oxidase is important for survival of Mycobacterium smegmatis under peroxide and antibiotic-induced stress, Sci. Rep. 5 (2015) 10333. https://doi.org/10.1038/srep10333.

C.J. Beebout, L.A. Sominsky, A.R. Eberly, et al., Cytochrome bd promotes Escherichia coli biofilm antibiotic tolerance by regulating accumulation of noxious chemicals, NPJ Biofilms Microbiomes. 7(1) (2021) 35. https://doi.org/10.1038/s41522-021-00210-x.

L. Léger, A. Budin-Verneuil, M. Cacaci, et al., β-Lactam exposure triggers reactive oxygen species formation in *Enterococcus faecalis* via the respiratory Chain component DMK, Cell Rep. 29(8) (2019) 2184-2191.e3. https://doi.org/10.1016/j.celrep.2019.10.080.

S. Kumar, K. Sandeep, R. Kumar, et al., Antimicrobial effect of pimozide by targeting ROS-mediated killing in *Staphylococcus aureus*, Biotechnol. Appl. Biochem. 70(5) (2023) 1679-1689. https://doi.org/10.1002/bab.2465.

R. Du, X. Li, Y. Xu, et al., Metagenomics reveals potential antimicrobial peptides in Chinese baijiu fermentation, Food Microbiol. 134 (2026) 104918. https://doi.org/10.1016/j.fm.2025.104918.

F. Ermoli, C. Spahn, I. Sadhir, et al., Activation of the Yersinia type III secretion system induces large-scale spatial reorganization of chromosomal and virulence plasmid DNA, Cell Rep. 44(12) 2025 116592. https://doi.org/10.1016/j.celrep.2025.116592.

Q. Li, G. Kim, L. Jing, et al., Electrostatics-Based computational design and experimental analysis of buforin II antimicrobial peptide variants with increased DNA affinities, ACS Omega 8(37) (2023) 33701-33711. https://doi.org/10.1021/acsomega.3c04023.

U. Majeed, H. Majeed, A. Shafi, et al., DNA binding peptide CF-14 enhances bactericidal efficacy of eugenol/carvacrol nanoparticles to *Escherichia coli*, Food Chem. 429 (2023) 136861. https://doi.org/10.1016/j.foodchem.2023.136861.

B. Gray, P. Hall, H. Gresham, Targeting agr- and agr-Like quorum sensing systems for development of common therapeutics to treat multiple gram-positive bacterial infections, Sensors (Basel) 13(4) (2013) 5130-5166. https://doi.org/10.3390/s130405130.

N.H. Mahdally, R.F. George, M.T. Kashef, et al., Staquorsin: A novel *Staphylococcus aureus* Agr-mediated quorum sensing inhibitor impairing virulence in vivo without notable resistance development, Front. Microbiol. 12 (2021) 700494. https://doi.org/10.3389/fmicb.2021.700494.

E. Geisinger, R.P. Adhikari, R. Jin, et al., Inhibition of rot translation by RNAIII, a key feature of agr function, Mol. Microbiol. 61(4) (2006) 1038-48. https://doi.org/10.1111/j.1365-2958.2006.05292.x.

J. Yan, B.L. Bassler, Surviving as a community: Antibiotic tolerance and persistence in bacterial biofilms, Cell Host Microbe. 26(1) (2019) 15-21. https://doi.org/10.1016/j.chom.2019.06.002.

X. Wan, Y. Wu, C. Zhang, Z. Yu, Z. Luo, Sub-minimum inhibitory concentrations of fosfomycin enhance *Staphylococcus aureus* virulence through the agr-PSM pathway, Microb Pathog. 210 (2026) 108138. https://doi.org/10.1016/j.micpath.2025.108138

S.E. Cramton, C. Gerke, N.F. Schnell, et al., The intercellular adhesion (*ica*) locus is present in *Staphylococcus aureus* and is required for biofilm formation, Infect. Immun. 67(10) (1999) 5427-5433. https://doi.org/10.1128/IAI.67.10.5427-5433.1999.

Q. Peng, X. Tang, W. Dong, et al., A review of biofilm formation of *Staphylococcus aureus* and its regulation mechanism, Antibiotics (Basel) 12(1) (2022) 12. https://doi.org/0.3390/antibiotics12010012.

J.M. Yarwood, D.J. Bartels, E.M. Volper, et al., Quorum sensing in *Staphylococcus aureus* biofilms, J. Bacteriol. 186(6) (2004) 1838-1850. https://doi.org/10.1128/JB.186.6.1838-1850.2004.

B.R. Boles, A.R. Horswill, Agr-mediated dispersal of *Staphylococcus aureus* biofilms, PLoS Pathog. 4(4) (2008) e1000052. https://doi.org/10.1371/journal.ppat.1000052.

J.W. Zhou, K.Y. Yin, W.Q. Luo, et al., Anti-virulence potential of carvone against *Serratia marcescens*. Food & Medicine Homology 1 (2024) 9420001. https://doi.org/10.26599/FMH.2024.9420001.